Petroleum Science 19 (2022) 2227–2239

Contents lists available at ScienceDirect

Petroleum Science

journal homepage: www.keaipublishing.com/en/journals/petroleum-science

Original Paper

Numerical analysis of the hydraulic fracture communication modes in fracture-cavity reservoirs

Jia-Wei Kao [a, b], Shi-Ming Wei [a], Wen-Zhi Wang [a, c], Yan Jin [a, *]

[a] State Key Laboratory Petroleum Resources and Prospecting, China University of Petroleum, Beijing, 102249, China
[b] Sinopec Research Institute of Petroleum Engineering, Beijing, 102206, China
[c] CNPC Engineering Technology R&D Company Limited, Beijing, 102206, China

ARTICLE INFO

Article history:
Received 21 January 2022
Received in revised form
18 May 2022
Accepted 19 May 2022
Available online 25 May 2022

Edited by Yan-Hua Sun

Keywords:
Fracture-cavity carbonate formation
Hydraulic fracture propagation
Numerical simulation
Fracture-cave communication
Discontinuous discrete fracture model

ABSTRACT

The fracture-cavity carbonate reservoirs in the Tahe Oilfield in China are mainly exploited by fracturing. We need the hydraulic fractures to communicate with caves to create a flow channel. However, due to the existence of the fracture-cavity systems, the hydraulic fracture propagation morphology is complicated, while the propagation characteristics are not clear. To analyze the hydraulic fracture propagation in fracture-cavity carbonate formations, based on the discontinuous discrete fracture model, we developed a solid-seepage-freeflow coupled fracturing model for fracture-cavity formations, which can simulate the complex interaction behavior of fractures and caves. Based on the simulation results, we found the interaction rule between hydraulic fractures and fracture-cavity systems: the stress concentration around caves is the main factor that determines the fracture propagation path. Deflection due to stress concentration is usually not conducive to communication, while natural fractures distributed around caves could break the rejection action. Increasing the hydraulic energy in the hydraulic fracture can make fracture propagate directly and reduce the influence of deflection. The steering fracture formed by temporary plugging is beneficial to the communication of fracture-cavity systems in the non-principal stress direction. According to the simulation results of different fracture-cavity characteristics, we raised four optimization communication modes for fracture-cavity carbonate formation to provide references for fracturing optimization design and parameter optimization.

1. Introduction

The carbonate formation in the Tahe Oilfield, China, is a typical fracture-cavity carbonate reservoir. In recent years, the development of the Ordovician reservoir has achieved a great result, indicating a considerable oil and gas potential (Li 2017). The matrix of the carbonate reservoir is extremely dense, and due to the geological structure, the fluid in the formation is mainly distributed in the fracture-cavity systems (Li 2017; Liu et al. 2018). However, the distribution of fracture-cavity systems in carbonate formation has various shapes and sizes, which leads to a highly heterogeneous (Ford 1988; Loucks 1999). Due to the deeply buried depth and the complex geologic process, it is not easy to describe the distribution of fracture-cavity systems in Ordovician formation accurately (Luo et al. 2013; Kremlev et al. 2008). According to the field statistics, about 33% of wells could drill into a cave, which could be put into production directly, while the remaining wells need to hydraulic fracturing to build a flow channel to communicate these caves. The fracturing effect is restricted due to the complexity of the fracture-cavity carbonate reservoir, so how to make the hydraulic fractures communicate with more caves is the key to improving the fracturing effect.

In recent years, scholars carried out a series of studies of the propagation of hydraulic fractures. Keshavarzi et al. (2012) found that the propagation behavior of hydraulic fractures in unconventional reservoirs was mainly controlled by the stress field and the direction of natural fractures. Sesetty and Ghassemi (2012) studied the relationship between opening fracture, hydraulic fracture path, in-fracture pressure, and fracturing time by DDM. Wang et al. (2021) analyzed the relationship between temporary plugging method and complex fracture morphology. Feng et al. (2016, 2017) simulated of fluid loss and fluid-driven interface debonding

* Corresponding author.
E-mail address: jinyancup@163.com (Y. Jin).

https://doi.org/10.1016/j.petsci.2022.05.011

Nomenclature

$\boldsymbol{C}$	Elastic parameter
d_f	Fracture aperture, m
d_{f0}	Initial fracture aperture, m
E	Elasticity modulus, GPa
F_V	Physical force
g	Gravity coefficient, 9.8 m/s^2
$\boldsymbol{I}$	Unit tensor
k_1	Formation permeability, mD
k_2	Fracture permeability, mD
K_n	Normal stiffness of natural fractures, N/m
$\boldsymbol{n}$	Normal direction of the cave wall
$\boldsymbol{n}_\Gamma$	Normal direction of fracture wall
$\boldsymbol{n}_f^+$	Norm vector of fractures surface'+'
$\boldsymbol{n}_f^-$	Norm vector of fractures surface'-'
p_0	Initial fluid pressure, MPa
p_1	Fluid pressure in the formation, MPa
p_2	Fluid pressure in the fracture, MPa
p_3	Fluid pressure in cave, MPa
q_Γ	Fluid filtration quantity, m^3/s
Q_m	Flow quantity, m^3/s
r_b	Fluid conductivity, equal to 0.1
$\boldsymbol{S}$	Stress tensor
$\boldsymbol{S}_0$	Initial stress
$\overline{S}_1$	Average compression ratio, MPa^{-1}
u	Displacement, m
$\boldsymbol{u}_1$	Flow velocity in formation, m/s
$\boldsymbol{u}_2$	Flow velocity in fractures, m/s
$\boldsymbol{u}_3$	Flow velocity in caves, m/s
$\boldsymbol{u}_C$	Flow exchanging rate between cave and formation, m/s
$\boldsymbol{u}_f^+$	Displacements of fracture surface '+', m
$\boldsymbol{u}_f^-$	Displacements of fracture surface '-', m
α_β	Biot coefficient, equal to 0.3
$\boldsymbol{\varepsilon}$	Strain tensor
υ	Poisson's ratio
ρ	Fluid density, equal to 1 × 10^3 kg/m^3
μ	Fluid viscosity, m/s
χ_f	Fluid compressibility, equal to 4 × 10^{-10} MPa^{-1}
χ_{p1}	Rock compressibility, equal to 1 × 10^{-11} MPa^{-1}
ε_{p1}	Matrix porosity, equal to 5%
ε_{f2}	Fracture porosity, equal to 100%
Γ_f^+, Γ_f^-	Deformation domain of the fracture wall

mechanism in fracturing process. Tan et al. (2019, 2020, 2021) analyzed the complex hydraulic fracture morphology in bedding shale through experiments and XFEM-based CZM simulation methods.

For the interaction between fracture and cave, preliminary research achievements have also been obtained. Yang et al. studied the interaction between crack and hole defects in the two-dimensional plate by experiments (Yang et al. 2016) and numerical simulation (Yang et al. 2018); they found that the defect would attract the crack as it expanded. Liu et al. (2019a, 2019b) studied the interaction between hydraulic fractures and caves through physical model experiments, and they thought that large caves would stop the propagation of hydraulic fractures. Cheng et al. (2019) used the extended finite element method to simulate the interaction between a single fracture and a single cave. Wang et al. (2018) analyzed the interaction between hydraulic fracture and a cave by FEMM methods. Liu Z. et al. (*2019*) studied the influence of an empty cave on the hydraulic fracture expanding path by phase-field method and found the deflection and attraction effect of the cave on the fracture propagation path by simulation. Luo et al. (2020) analyzed the influence of a hole containing liquid on the fracture propagation path in a poroelasticity medium by XFEM.

Previous studies focused on the interaction between hydraulic fracture and a single circular cave. However, a series of caves with different sizes and shapes and natural fractures are distributed in fracture-cavity carbonate formation. We need to further study the propagation of hydraulic fractures in the above conditions.

In this paper, we built up the fracture-cavity carbonate geological models, in which ellipse caves with different sizes and shapes and natural fractures were distributed randomly. We simulated the hydraulic fracture propagation trajectory in fracture-cavity carbonate formation under different injection conditions and summarized the interaction between hydraulic fracture and fracture-cavity systems. Based on the results, we proposed four optimized methods to improve the communication effect between hydraulic fracture and fracture-cavity systems, according to the results. This research could give a better understanding of the propagation of hydraulic fractures in fracture-cavity carbonate formation.

2. Hydraulic fracture propagation model in fracture-cavity carbonate formation

Based on the discrete fracture model (Karimi-Fard et al. 2003; Garipov et al. 2016), we have built a discontinuous discrete fracture model (Wei et al. 2021) to realize hydraulic fracturing processes. Based on our previous work, we improved the discontinuous discrete fracture model, in which natural fractures and caves within fluid are added, and the solid-seepage-freeflow coupled process could be considered during hydraulic fracturing in fracture-cavity formation. By further adding and modifying grid nodes, we could simulate the complex interaction between hydraulic fractures and fractures and caves, such as deflection, connection, and penetration. This model is developed and realized in COMSOL and MATLAB.

2.1. Solid stress module

The rock matrix is set as a continuous porous elastomer, and the governing equation is as follows:

$$\boldsymbol{S} = \boldsymbol{S}_0 - \alpha_\beta p_1 \boldsymbol{I} + \boldsymbol{C} : \boldsymbol{\varepsilon}, \tag{1}$$

$$\boldsymbol{C} = C(E, \upsilon), \tag{2}$$

The strain tensor under the continuum hypothesis is characterized by displacement:

$$\boldsymbol{\varepsilon} = \frac{1}{2}\left(\nabla u + \nabla^{\mathrm{T}} u\right), \tag{3}$$

The quasi-static momentum conservation equation of elastic formation with saturated pores is as follow:

$$0 = \nabla \cdot (\boldsymbol{S}_0 - \alpha_\beta p_1 \boldsymbol{I}) + \boldsymbol{F}_V, \tag{4}$$

2.2. Flow module

This model assumes that injection fluid and formation fluid are the same, and there is no phase transition during fracturing. This study focuses on fracture propagation and the interaction behavior between hydraulic fracture and fracture-cavity systems, so we simplify the initiation process from the wellbore, and an initial hydraulic fracture is set instead in the middle. Therefore, we need to pay attention to fluid flow in fracture systems, fluid flow in caves, and mass transfer processes between them, as shown in Fig. 1, and adopt appropriate equations to describe these processes.

We use Darcy's law to describe slow flow in the formation caused by pressure difference:

$$\frac{\partial}{\partial t}(\varepsilon_{p1}\rho) + \nabla\cdot(\rho \boldsymbol{u}_1) = Q_m, \tag{5}$$

$$\boldsymbol{u}_1 = -\frac{k_1}{\mu}\nabla p_1, \tag{6}$$

We assume the fluid had weak compressibility. The pressure change caused by fluid flow leads to the volume change of formation, including rock and fluid in pores. Therefore, the mass conservation equation is expressed as follows:

$$\bar{S}_1 = \varepsilon_{p1}\chi_f + (1-\varepsilon_{p1})\chi_{p1}, \tag{7}$$

$$\frac{\partial}{\partial t}(\varepsilon_{p1}\rho) = \rho\bar{S}_1\frac{\partial p_1}{\partial t}, \tag{8}$$

The flow in the hydraulic fracture can always be simplified as a channel flow along the fracture length direction (Guo et al. 2015), as the length of the hydraulic fracture is several orders of magnitude higher than the width. This process is described as the fracture flow:

$$d_f\frac{\partial}{\partial t}\left(\varepsilon_{f2}\rho\right) + \nabla_T\cdot\left(d_f\rho\boldsymbol{u}_2\right) = d_f Q_m, \tag{9}$$

$$\boldsymbol{u}_2 = -\frac{k_2}{\mu}\nabla_T p_2, \tag{10}$$

$$k_2 = d_f{}^2/12, \tag{11}$$

The fracture aperture is controlled by pore pressure (Xia et al. 2015) and the action of the in-situ stress field, as shown in Fig. 2:

$$d_f = d_{f0} - \left(\boldsymbol{u}_f^+\cdot\boldsymbol{n}_f^+ + \boldsymbol{u}_f^-\cdot\boldsymbol{n}_f^-\right), \tag{12}$$

Fluid filtration from fracture to formation is along the normal direction of the fracture surface.

$$-2\rho\frac{k_1}{\mu}\boldsymbol{n}_\Gamma\cdot\nabla p = -q_\Gamma, \tag{13}$$

To simulate the free flow of fluid more realistically in caves, we use the N–S equations of the slightly compressible fluid to describe the flow in caves (Wei et al. 2020):

$$\frac{\partial\boldsymbol{u}_3}{\partial t} + \boldsymbol{u}_3\cdot\nabla\boldsymbol{u}_3 = -\frac{1}{\rho}\nabla p_3 + \frac{1}{3}\frac{\boldsymbol{u}_3}{\rho}\nabla(\nabla\cdot\boldsymbol{u}_3) + \frac{\mu}{\rho}\nabla^2\boldsymbol{u}_3, \tag{14}$$

For Eq. (14), $\boldsymbol{u}_3$ and p_3 are needed to be solved, in an enclosed system, the continuity equation is applied as:

$$\frac{\partial\rho}{\partial t} + \nabla\cdot(\rho\boldsymbol{u}_3) = 0, \tag{15}$$

The compressibility of the fluid in the caves should also be considered:

$$\rho = \rho_0\left[1 + \chi_f(p_3 - p_0)\right], \tag{16}$$

During hydraulic fracturing, formation pressure changes due to the filtration from hydraulic fracture to formation, and formation fluid will exchange with the fluid in cave under pressure difference. We describe fluid exchange occurred in the normal direction of caves' walls by a permeable layer model:

$$-\boldsymbol{n}\cdot\rho\boldsymbol{u}_C = \rho r_b\left(\frac{p_3 - p_1}{\rho g}\right), \tag{17}$$

2.3. Hydraulic fracture propagation module

In previous work, we built a discontinuous discrete fracture model to simulate fracture propagation (Wei et al. 2021). This model constructed discrete fractures based on DFM, while in solid-fluid coupling stress field calculation, the solid module and the fluid module use the common nodes. The model allows hydraulic fractures to expand along the initial grid lines, and the minimum strain

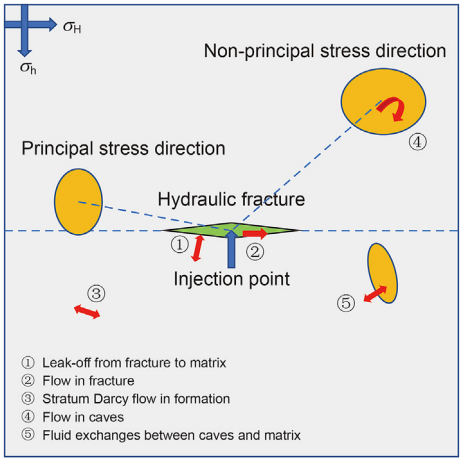

Fig. 1. Schematic diagram of flow module.

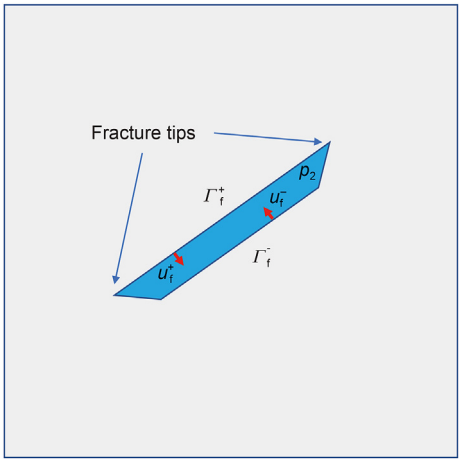

Fig. 2. The mechanics model of the fracture.

energy density criterion (Sih 1974) is adopted as the propagation criterion, and fracture propagation is orderly and gradual, as shown in Fig. 3.

In a fracture-cavity carbonate formation, fractures and caves are developed, the hydraulic fracture will show different propagation behavior when intersecting with them. We need special treatment for grid nodes when the hydraulic fracture intersects with natural fractures and cavities. This model assumes that all natural fractures have a low aperture at the initial stage, so the double fracture surfaces are simplified as closed while displacement is continuous. These closed fractures could be activated under the influence of hydraulic fractures, and discontinuous displacement occurs. When the hydraulic fracture tip reaches the natural fracture, we still use the energy method to determine the optimal propagation path. According to the different propagation paths, such as penetration and deflection, the intersection of hydraulic fracture and natural fracture should follow different mesh processing methods, as shown in Fig. 4.

When the hydraulic fracture communicates with a cave, the fracture will disrupt the continuity of cave wall; therefore, we carry out an additional separation treatment for the intersection nodes to ensure rationality to achieve the discontinuous coordination of displacement between fracture and cave. As the fluid injection continues, the fluid pressure in cave increases; when cave wall matrix meets the maximum circumferential stress failure criterion, a new hydraulic fracture will generate and extend. Thus, the fracture completes the penetration of cave, and this process also requires a node addition operation for cross point, as shown in Fig. 5.

3. Results and analysis

3.1. Model validation

To verify the correctness of the model built in this paper, especially for the accuracy of the simulation analysis results of the interaction between fractures and fracture-cavity systems, we selected two physical fracturing experiments for comparison and verification.

To determine the location, number, and size of fractures and caves in the specimens accurately, we manufactured artificial rock samples within prefabricated caves and fractures. Eight caves were located around the wellbore in specimens, and 12 vertical natural fractures were distributed at the same height as caves, as shown in Fig. 6. By adjusting the ratio of lime and sand and binder strength, we could make the artificial specimens are close to natural limestone in strength and elastic properties.

The loading conditions are shown in Table 1. Under reverse fault stress conditions, hydraulic fractures initiated perpendicular to the minimum horizontal stress direction, and propagated along the maximum horizontal stress direction, then interact with fractures and caves. After experiments, we opened specimens to observe fracture morphologies. To display results comprehensively, we reconstructed them according to the experimental results, as shown in Fig. 7.

Experimental results showed that in specimen 1 with a low injection rate, the fracture propagated to a certain deflection angle and intersected a natural fracture on the left side, while no cave communicated; in specimen 2 with a high injection rate, deflection angle decreased, and a cave communicated on the left.

According to the above results, we raised a compared simulation work based on the model built in this paper. We used the same stress and injection conditions in experiments and in simulations, and the results are shown in Fig. 8.

Simulation results showed that under low injection rate conditions, fracture propagation was deflected, failing to communicate with caves ahead. In contrast, for high injection rate, the hydraulic fracture expanded forward and communicates with caves in front. The consistency between simulation and experimental results showed the model accuracy in simulating fracture propagation in fracture-cavity formation.

3.2. Model setting and simulation parameters

According to the distribution characteristics of the fracture-cavity system in the Tahe Oilfield, as shown in Table 2, we establish geological models of fracture-cavity carbonate. The models are 160 m or 100 m squares, and the height is set as 10 m (Straight wells are always drilled in deep carbonate formations). Caves and fractures of different sizes and shapes are randomly distributed and not connected. As the fracture initiation from the wellbore is ignored, we directly set an initial hydraulic fracture in the center, with a half-length of 1.5 m and along the direction of the horizontal maximum *in-situ* stress. Hydraulic fractures start propagating directly from the initial fracture.

In this section, we simulate the hydraulic fracture in fracture-cavity carbonate formation under different injection conditions. Then we analyze the improvement effect of temporary plugging and steering fracturing on fracture-cave communication. There are eight simulation cases divided into two types: one is a 160-m square model, in which 12 caves with random position, shape, and size are distributed; the other is a 100-m square model, with eight random caves and several natural fractures distributed, as shown in Table 3.

We adopt unified fracturing parameters for simulation in these cases, as Group 1 (the basic group). Following that, we change the injection parameters (fracturing injection rate and injection fluid viscosity) and analyze the variation of the propagation rule, as Group 2 and 3. The simulation parameters are shown in Table 4. In

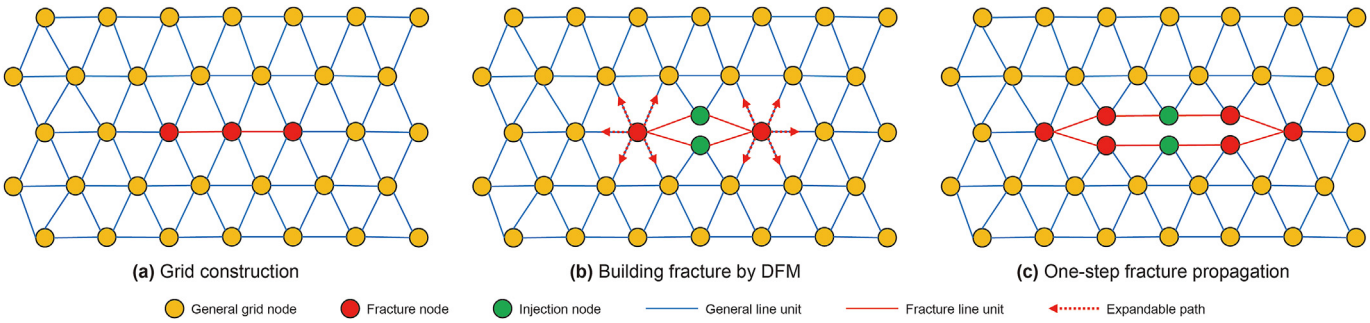

Fig. 3. Hydraulic fracture propagation method in the discontinuous discrete fracture model.

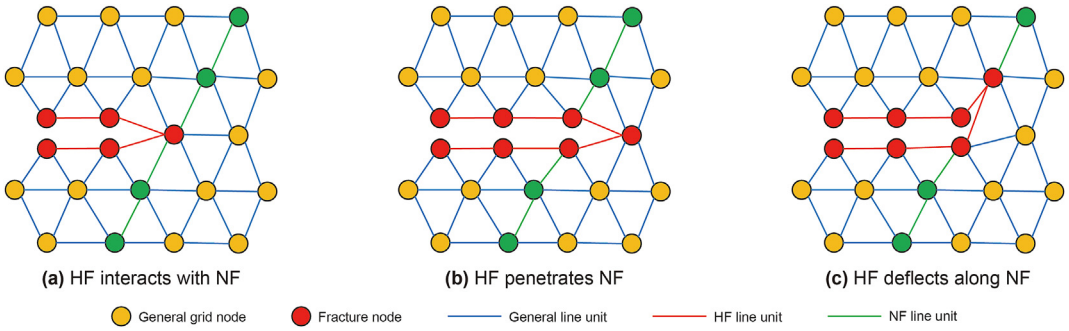

Fig. 4. Grid treatment method for the intersection of hydraulic fracture (HF) and natural fracture (NF).

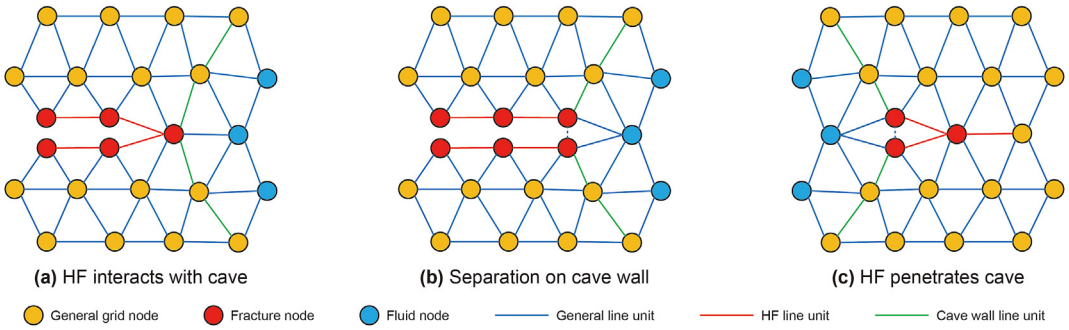

Fig. 5. Grid treatment method for the intersection of hydraulic fracture (HF) and cave.

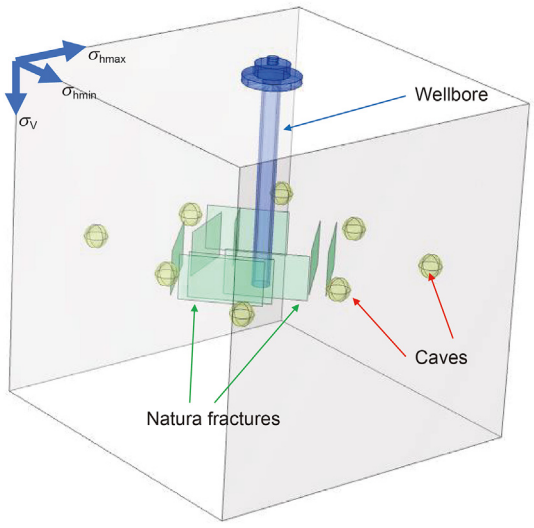

Fig. 6. Physical fracturing experiment specimen for fractured-cavity formation.

Table 1
Experimental conditions.

Specimen	$\sigma_V/\sigma_{Hmax}/\sigma_{hmin}$, MPa	Injection rate, mL/min	Viscosity, mPa s
Specimen 1	20/15/7	5	10
Specimen 2	20/15/7	20	10

addition, we select one case from each group to simulate the temporary plugging steering fracturing based on the first fracturing, as Group 4.

The distribution of fracture-cavity systems in eight cases and the direction of the local maximum principal stress in the initial state are shown in Fig. 9. From the initial stress distribution, we know that the direction of the local maximum stress and the horizontal maximum ground stress are almost the same; however, there is stress concentration around caves, which leads to the local maximum stress direction around disturbed, as a form of circumventing the caves. Moreover, the direction of the principal stress distribution is complicated due to the multi-caves disturbance.

It should be noted that we allow all the fractures to penetrate the caves as if they connect in order to observe the whole fracture propagation morphologies.

3.3. Simulation results

Group 1: We set the injection rate and viscosity at an average level in the first group. According to the results shown in Fig. 10, hydraulic fractures show different morphologies due to the different distribution of fracture-cavity systems. As can be seen from comparing different types of fracture-cavity systems, the communication effect is relatively poor in cavernous formation (the first four cases). For example, in simulation cases 2-1# and 3-1#, the hydraulic fracture does not communicate to any cave, while in the other two, only in case 1-1# caves are communicated. In contrast, in the fracture-cavity formation (cases 5#–8#), the communication effect is significantly improved; only one natural fracture and no cave were communicated in case 7#; while in the other three cases, hydraulic fractures are all intersected with fractures and caves.

The simulation results show a typical phenomenon that needed to be emphasized with the local maximum stress direction before fracturing (Fig. 9). First, the initial maximum principal stress direction should show a surrounding distribution around the caves. Then during fracturing, hydraulic fractures will propagate along the direction of the horizontal maximum *in-situ* stress. However, when

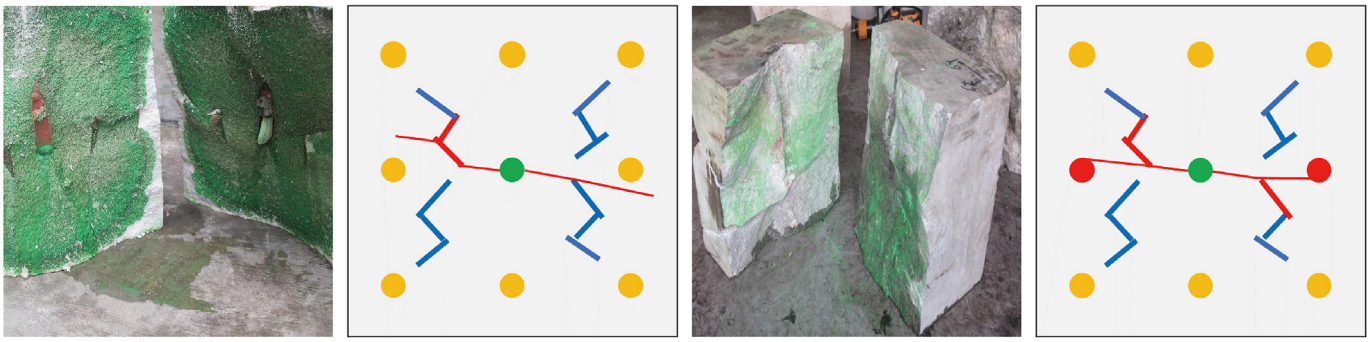

Fig. 7. Results and reconstruction of physical fracturing experiments.

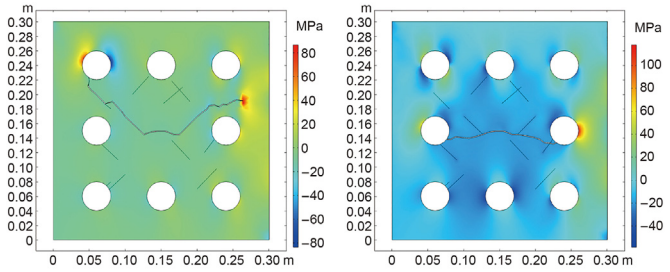

Fig. 8. Simulation results of fracture-cave fracturing experiment.

Table 2
Basic parameters of fracture-cavity carbonate formation model.

Parameter	Value
$\sigma_{Hmax}/\sigma_{hmin}$, MPa	110/90
Formation pressure, MPa	68
Matrix permeability, μm^2	0.01×10^{-3}
The proportion of the total area of caves, m^2	>2%
Matrix porosity	5%
Elasticity modulus, GPa	39
Poisson's ratio	0.26
The initial width of hydraulic fracture, mm	2
Biot coefficient	0.3

Table 3
Basic information of 8 cases.

Case No.	Model size	Cave number	Fracture number
1	160	12	0
2	160	12	0
3	160	12	0
4	160	12	0
5	100	8	16
6	100	8	16
7	100	8	24
8	100	8	24

fractures approach the caves, they are affected by the local stress concentration around the cave, and the propagation directions are deflected. While the deflection direction of the fracture is often close to the direction of the local maximum stress, which makes the fracture tend to bypass the cave. We define this deflection as the repulsion of the caves to the fractures, while the larger the cave is, the more pronounced the repulsion is. For example, in cases 3-1#, 6-1#, and 7-1#, when the fractures approach the caves in front, they all deflect as the rule described above and ultimately fail to communicate.

But such a deflection caused by the stress concentration around the cave does not necessarily lead the fracture to bypass the cave. Due to the existence of several caves, the local principal stress distribution around is complex; besides, when fractures approach the caves, the stress distribution will be further disturbed, which increases the complexity of the stress disturbance. Even so, fractures will still tend to expand along the direction of the maximum local ground stress around the fracture tip. As a result, the caves in the principal stress direction repel the fracture to some extent but can still communicate; by contrast, the caves in the non-principal stress direction are difficult to communicate.

Group 2: In this group, the injection rate is increased from 3 to 8 m^3/min, and the simulation results are shown in Fig. 11.

Compared with the results of the first group, we see that the deflection path of the fracture disturbed by the caves decreases significantly. Hydraulic fractures are more inclined to expand along the initial prefabricated direction (i.e., the direction of the horizontal maximum *in-situ* stress). As the deflection of the fractures decreases, hydraulic fractures communicate caves in front; however, bypass in Group 1. For example, in cases 6-2# and 7-2#, the caves located on the left of the infusion point are communicated in Group 2. In case 3-2#, the fracture propagates and communicates with the second cave after penetrating the first cave.

The increase in the injection rate can cause the fracture a higher net pressure at the same length, which plays a leading role in determining the fracture propagation direction. The increased net pressure can reduce the influence of stress concentration around caves and reduce the fracture deflection degree. At the same time,

Table 4
Injection parameters in four groups.

Fracturing parameters	Viscosity, mPa s	Injection rate, m^3/min
Group 1: Basic cases	30	3
Group 2: Change in injection rate	30	8
Group 3: Change in viscosity	6	3
Group 4: Temporary plugging steering fracturing	Same to the first fracturing	

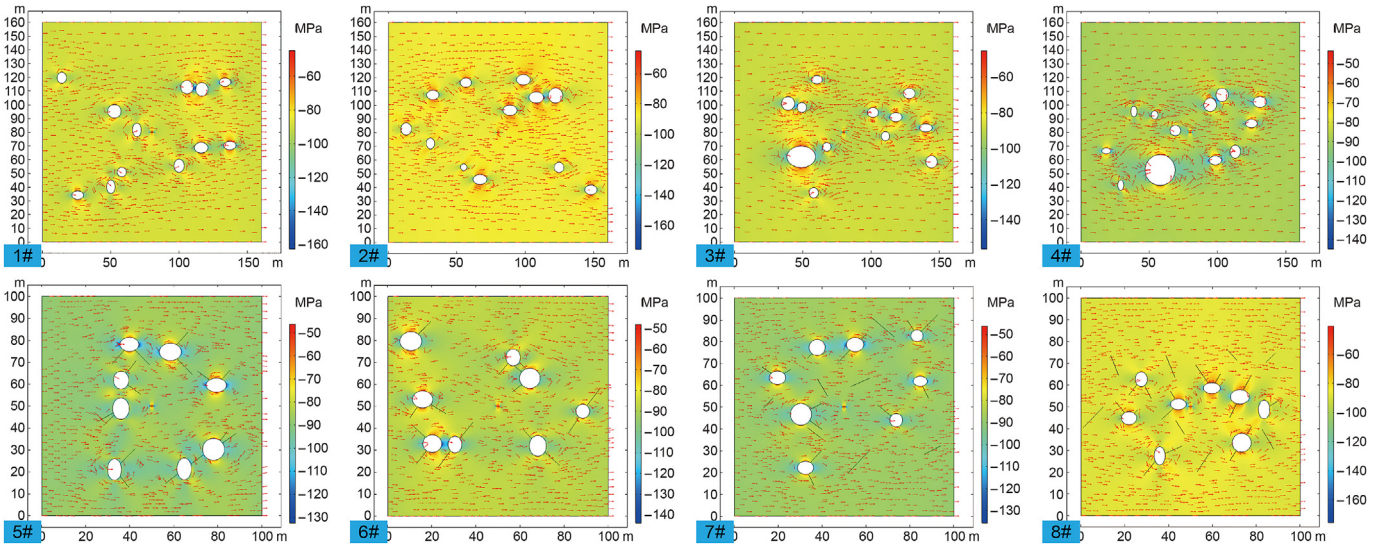

Fig. 9. Distribution of fracture-cavity systems and the initial local maximum stress field.

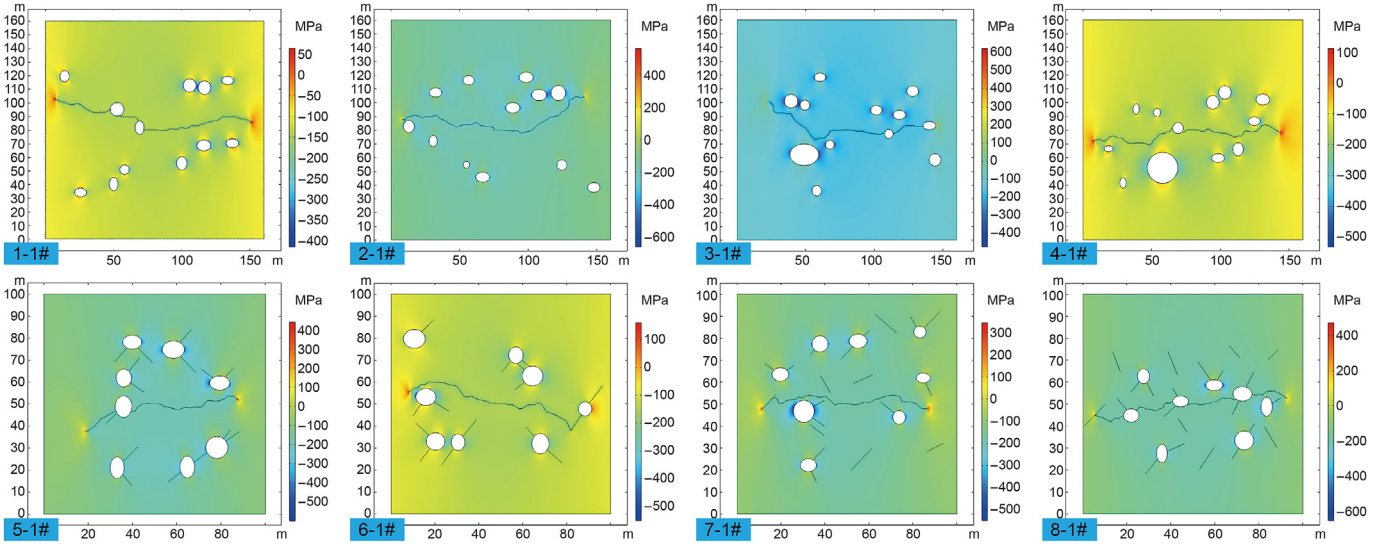

Fig. 10. Simulation results of Group 1.

however, it should be noted that the pressures at the injection point are much higher than in the first group. The flow friction increases under a high flow rate, which needs a higher pressure to break the cave wall. The injection rate should be limited if there is a pressure threshold in wellhead equipment during fracturing.

Group 3: In this group, we reduce the viscosity of the injection fluid from 30 to 6 mPa s. The results are in Fig. 12.

We find some differences in the fracture propagation trajectory compared with the first group, but not great as that between the first and second groups. As the viscosity of the injection fluid decreases, the frictional resistance of the fluid flow within the fracture decreases, so the net pressure within the fracture in Group 3 is higher than in Group 1. The fractures can resist deflection around the cave to a certain extent but not completely play the dominant role. Like case 4-3#, fractures still show a deflection similar to case 4-1#; in case 5, it can be seen from the deflection amount of the left fracture is Group 1 > Group 3 > Group 2.

The injection point pressures required for hydraulic fractures to penetrate the same cave are lower than those in Group 1. It indicates that low viscosity is conducive to the hydraulic energy transmission within fractures, and the fracture penetration ability is improved.

Group 4: Although we can overcome the rejection of the caves by increasing the injection rate and reducing the viscosity, hydraulic fractures can still only communicate with the caves in the principal stress direction. However, it is not easy for fracture-caves in non-principal stress direction to be communicated by one-time fracturing. Thus, in Group 4, we raise temporary plugging steering fracturing based on the first-time fracturing results in eight simulations cases (1–3#, 2-1#, 3-3#, 4-1#, 5-2#, 6-2#, 7-1# and 8-1#). The first hydraulic fractures are temporarily plugged at the entrance, and new fractures initiate at the injection point from the vertical direction. This group also simplifies the steering fracture initiation analysis after temporary plugging; the steering fractures are prefabricated perpendicular to the first-time fracture.

We assume that the temporary plugging breakthrough pressure

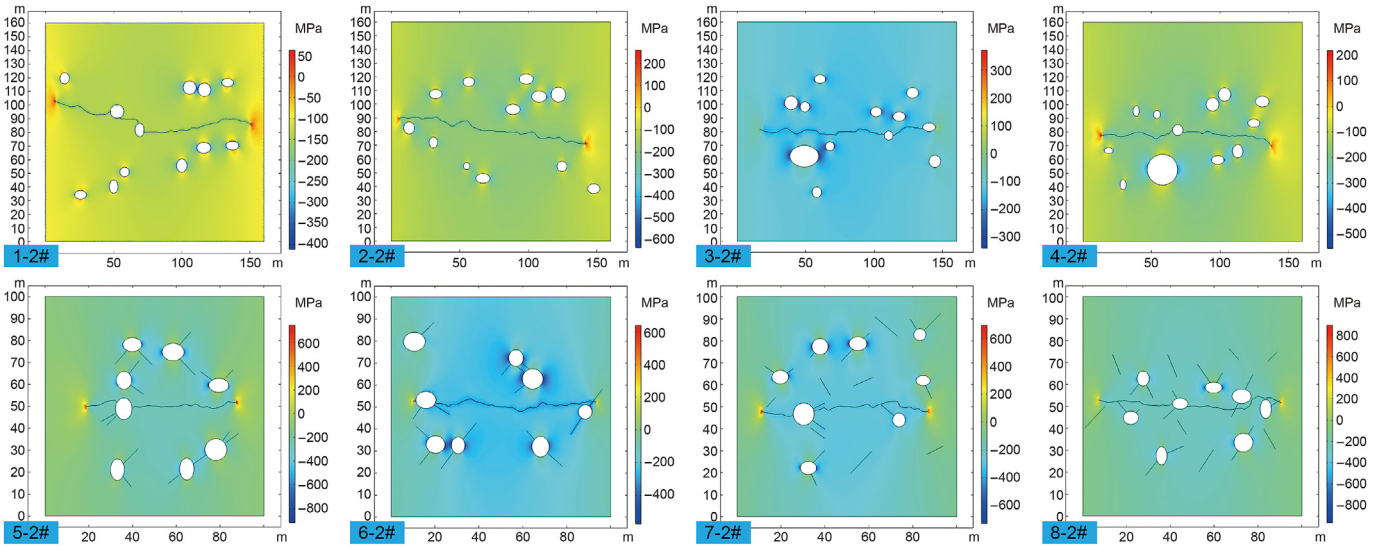

Fig. 11. Simulation results of Group 2.

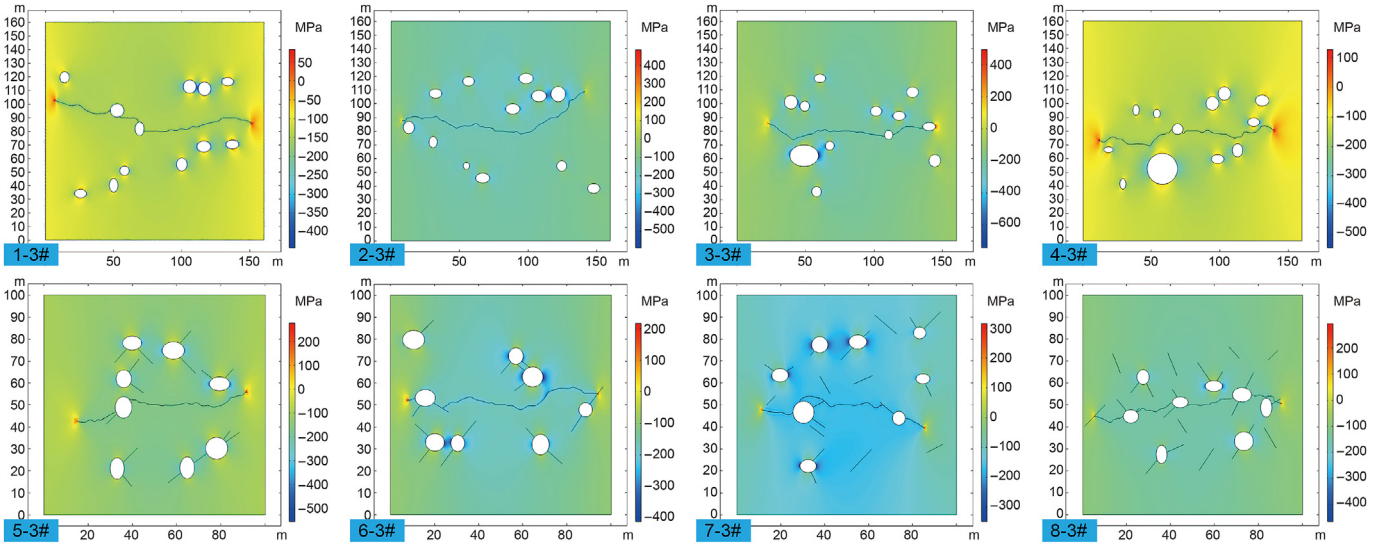

Fig. 12. Simulation results of Group 3.

is 20 MPa; when the fluid pressure at the entrance minus minimum *in-situ* stress reaches 20 MPa, the temporary plugging fails; or if the steering fracture intersects the first-time fracture, the steering fracturing stops.

As shown in Fig. 13, in the steering simulation of case R1-3#, the fracture begins to deflect after expanding by about 10 m along the initial direction. Then the upper steering fracture communicates with the fracture-cavity system of first-time fracturing, which leads to the stop of steering fracturing. The fractures on the lower side fail to communicate with a new cave. The same phenomenon occurred in the steering fracturing simulation of case R3-3# and case R8-1#. In the simulation of case R2-1#, the upper steering fracture communicates two caves successively, while the lower fracture does not communicate one. For case R4-1#, the steering fractures on the upper and lower sides communicate with caves with two and one, respectively. In cases R5-2# and R6-2#, the steering fractures communicate fracture-cavity systems by intersecting natural fractures around caves.

In steering fracturing, the fracture propagation ability is limited by the temporary plugging pressure of the first-time fracturing. Therefore, it is challenging to have a large propagation capacity compared with the first hydraulic fracturing, and the ability to penetrate the cave is limited. Steering fracturing is more effective in fracture-cavity formations than in cavernous formations because it is easier for the steering fractures to communicate with caves by activating natural fractures around them.

The simulation results in this group show that it is possible to communicate with new caves by steering fracturing to improve the fracturing effect of cavernous carbonate reservoirs. Therefore, it is worth further studying the diversion fracturing technology and enhancing the effect of fracture-cavity communication.

3.4. Interaction between hydraulic fracture and fracture-cavity systems

Based on the simulation results, the hydraulic fracture

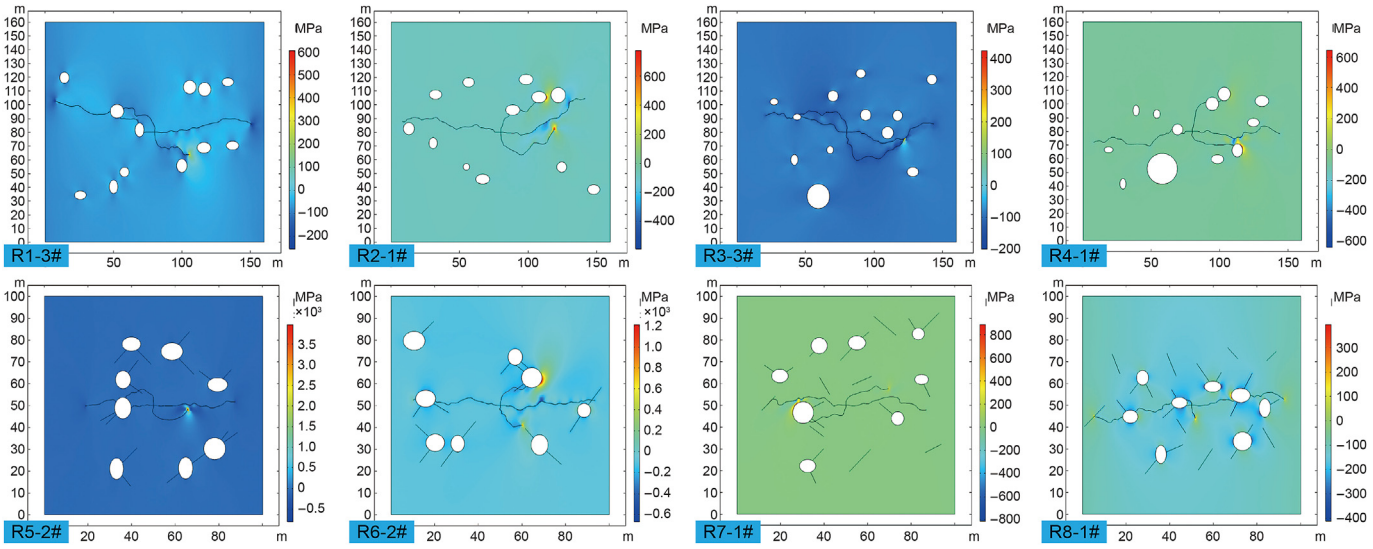

Fig. 13. Simulation results of Group 4.

propagation rules in fracture-cavity carbonate reservoirs are summarized:

(1) In general, the hydraulic fracture interacts with the fracture-cavity systems in the principal direction, as shown in Fig. 14. From the above simulation results, we can see that hydraulic fractures always expand along the direction of the maximum horizontal principal stress. Only when there are fracture-cavity systems developed in front of the propagation direction can they interact with each other and communicate. The fracture-cavity systems in the non-principal stress direction have less influence on fracture propagation and are challenging to communicate.

(2) When the hydraulic fracture expands and approaches a single cave, repulsion in the positive direction or attraction in the lateral direction will occur according to the different relative positions. The local maximum stress distribution around the caves could divide into two cases: the "Around cave" pattern and the "Pointing to cave" patterns, according to the relative size of the fluid pressure in caves, as shown in Fig. 15.

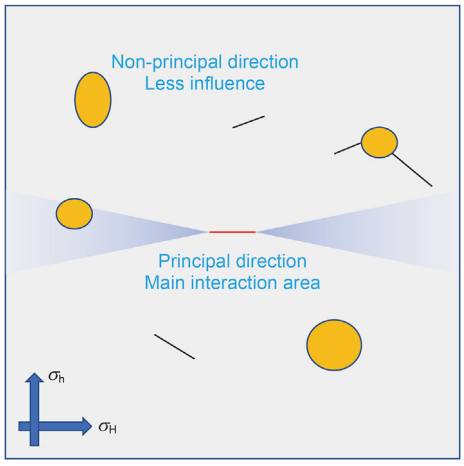

Fig. 14. Interaction between hydraulic fracture and fracture-cavity systems in different directions.

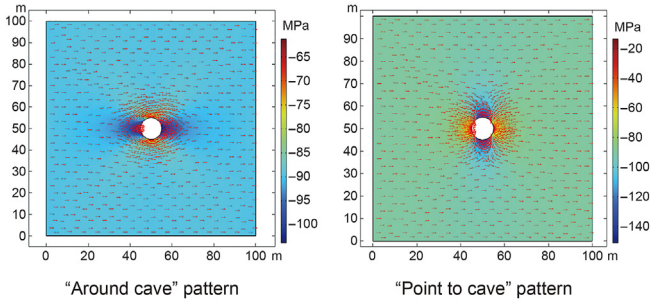

Fig. 15. The local maximum stress distribution around caves under different in-cave fluid pressures.

When the hydraulic fracture approaches the cave from the front, it will deflect to the side under the influence of the stress disturbance around the cave, showing a rejection result; on the contrary, the hydraulic fracture approaches the cave from the lateral, it will be attracted to the cave, showing an attraction result, as shown in Fig. 16. Although hydraulic fractures intersect caves with different deflection characteristics due to different relative positions, hydraulic fractures are deflected along the direction of local maximum principal stress due to the effect of stress concentration around caves.

(3) When multiple caves are close, stress disturbance will appear around caves, resulting in a complicated stress distribution characteristic. At this time, hydraulic fractures would show a variety of complex behavior when interacting with multi-caves, which are influenced by the number of caves, relative position, and morphology. As shown in Fig. 17, three typical features are as follows:

a. Caves are close to each other, while when the hydraulic fracture is on one side, it will bypass multi-caves, which can be regarded as a single large cave;
b. The hydraulic fracture expands along the path with the lowest strain energy between caves and bypasses them;
c. After the first cave is penetrated, the hydraulic fracture continues to interact with the second one. However, whether it could communicate the second cave is affected by various

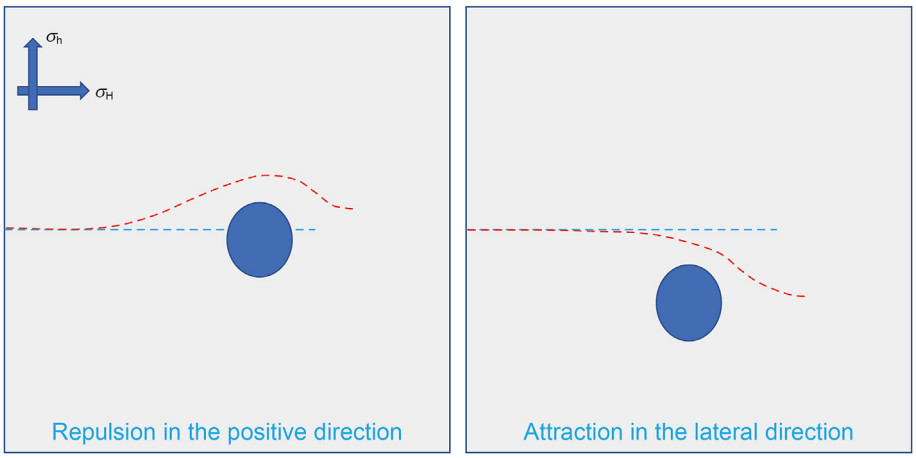

Fig. 16. Repulsion in the positive direction and attraction in the lateral direction.

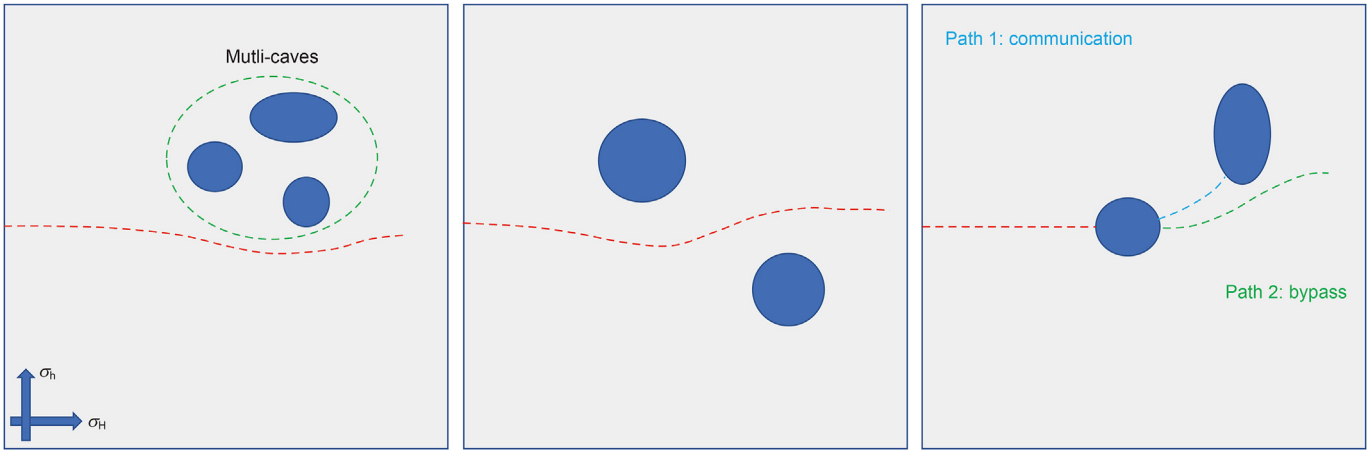

Fig. 17. Typical features of the hydraulic fracture interacting with multi-caves.

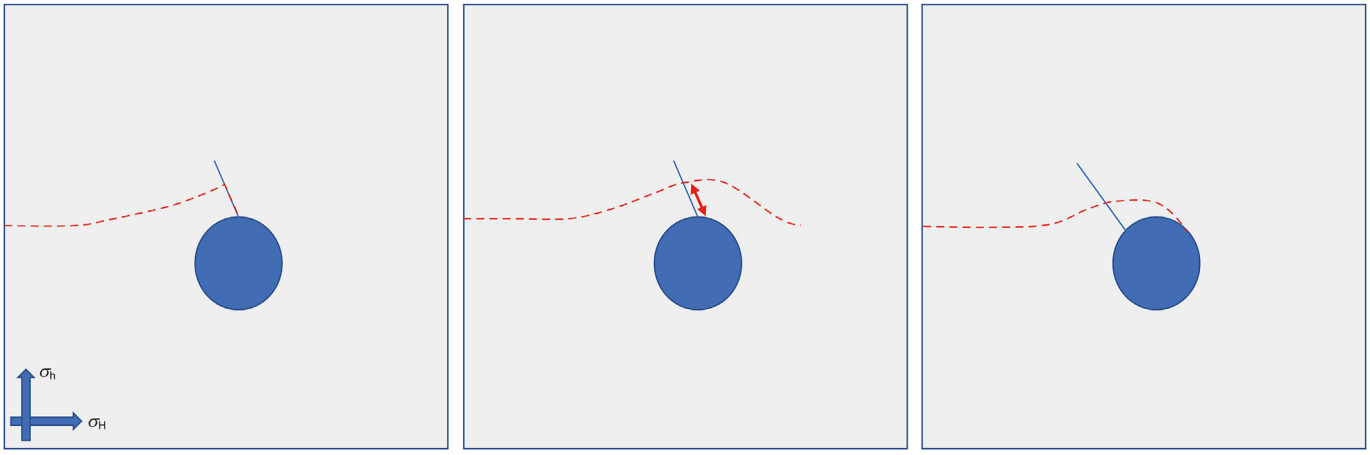

Fig. 18. Interaction behavior between the hydraulic fracture and the fracture-cavity system.

factors such as the relative position, distance, and hydraulic energy, which always needs specific analysis.

(4) When the hydraulic fracture interacts with a fracture-cavity system, we observe three unique characteristics, as shown in Fig. 18:

a. The hydraulic fracture turns into the cave by the natural fracture around;
b. The hydraulic fracture bypasses the cave but communicates by activating natural fracture;

c. The hydraulic fracture penetrates the natural fracture around the cave and then deflects towards the cave and connects, as the fluid pressure in the cave rises due to the injection, which changes the local maximum stress distribution around the cave from the "Around cave" pattern to the "Pointing to cave" pattern.

We can see when the hydraulic fracture interacts with a fracture-cavity system, it still deflects due to stress concentration. However, due to the existence of the natural fracture around, the hydraulic fracture can establish a flow channel to connect the cave after intersection, to reduce communication difficulty.

(5) The degree of propagation deflection of the hydraulic fracture decreases with the increase in net fluid pressure, which is conducive to breaking through the repulsion of the cave in front and improving the communication effect, as shown in Fig. 19. In the simulation, we find that in those cases with high pressure in a fracture, the deflection degree of the hydraulic fracture is significantly reduced, and it is more inclined to expand directly along the initial direction. From the perspective of strain energy, we know that when the pressure in the fracture increases, the fluid applies greater compressive stress on the fracture wall, which leads to a higher strain energy density; however, this compression action could lead to a tensile stress action of rock matrix in front of fracture tip in the same direction and results in a decrease in strain energy density in this region. Therefore, the hydraulic fracture tends to expand in the existing direction. The net fluid pressure in the fracture is a key parameter in fracturing, and it is also controllable. We need to study further the influence of fluid pressure in the fracture on fracture-cave interaction.

3.5. The optimization fracturing communication mode for the fracture-cavity reservoir

Based on the above simulation analysis, we propose the following four optimization fracturing modes for fracture-cavity carbonate reservoirs, aiming at the formations with different fracture and cave characteristics, as shown in Fig. 20:

(1) Strong penetration mode for caves in the principal stress direction. For the cavernous carbonate reservoirs with no fracture development, the main target should be the hydraulic fracture communicating with caves in the main stress direction. By adjusting the injection parameters, we can improve the net pressure in the hydraulic fracture to break through the repulsion of caves in the principal stress direction and communicate them.

(2) Searching caves along fractures mode. For reservoirs with some fractures developed, we need to make use of the beneficial effect of fractures around caves on the communication between hydraulic fractures and fracture-cavity systems. The hydraulic fracture communicates with the fracture around the cave to establish a flow channel. In this mode, the communication difficulty is reduced, while the fracture-cavity system communication range is improved.

(3) Multi-fracture channel communication mode. In mode one and mode two, we use single fracturing to communicate the fractures in the direction of principal stress, while in this model, temporary plugging and diversion fracturing is suggested to build new fractures in the non-principal stress direction to communicate lateral cavities to develop the reservoir potential fully.

(4) Volume fracturing communication mode. For reservoirs with natural fractures well developed, we suggest volume fracturing to activate natural fractures to form complex fractures and then communicate fracture-cavity systems in multiple directions. Due to the energy determination method in the simulation in this paper, which does not allow fracture bifurcation, we do not carry corresponding simulations. While researchers (Liu et al. 2020) have given a clear conclusion by modeling experiments, they observed that hydraulic fractures form volume fractures through natural fractures and then communicate cavities in different directions, the communication effect is significantly improved.

4. Discussion

(1) Through simulation results, we find that the distribution of the local stress field in the cavernous carbonate reservoir is the main factor affecting the hydraulic fracture propagation. In the actual carbonate formation, there are also kinds of filling in the caves besides oil and water (Tan et al. 2011; Li 2017), which affect the stress distribution around caves to a certain extent. Moreover, the shape of fracture-cavity systems is actually more complicated; if the local stress field in the fracture-cavity carbonate reservoir can be evaluated

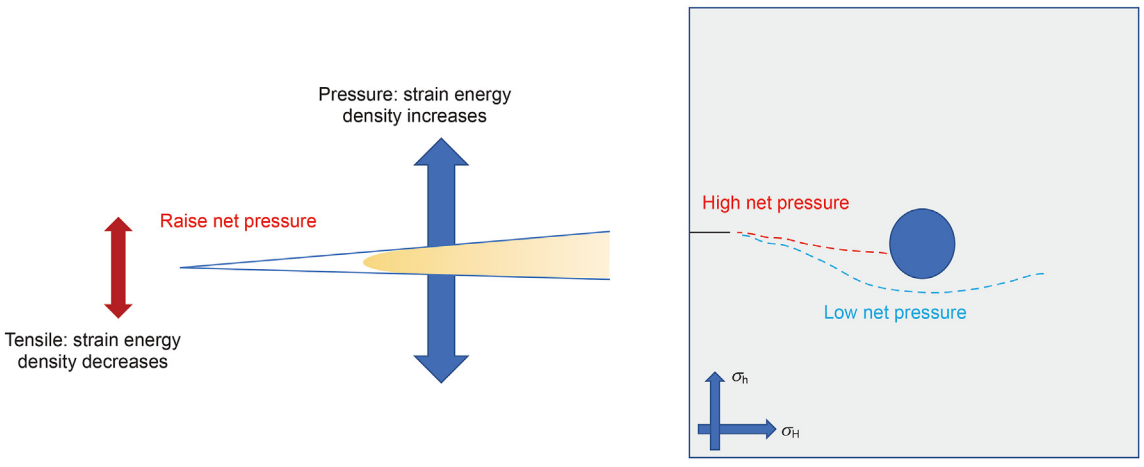

Fig. 19. Effect of net pressure in fracture on fracture-cave interaction.

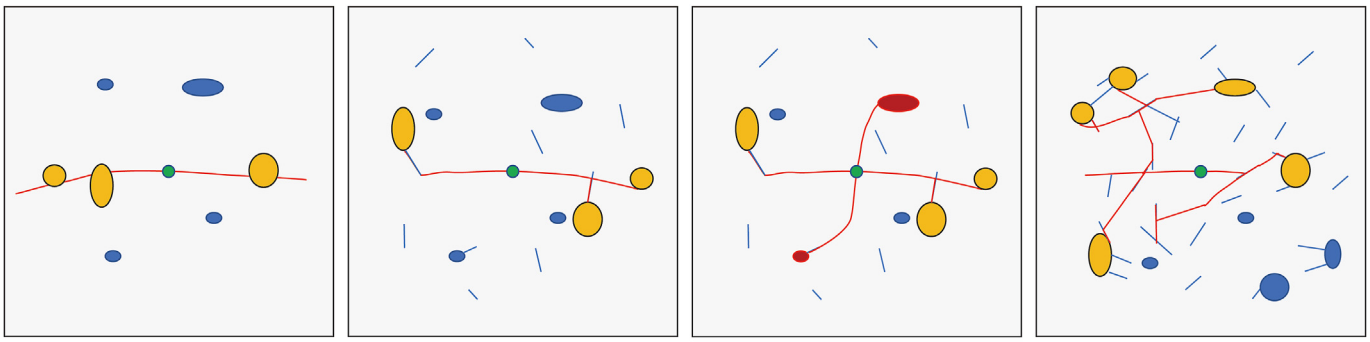

Fig. 20. Four optimization fracturing communication modes.

accurately, we will do better in fracturing design and process optimization.

(2) By adjusting fracturing engineering parameters (high injection rate and low viscosity fracturing fluid), we can increase the ability of hydraulic fractures to communicate caves in the principal stress direction. However, there may be some high leakage zones in the carbonate formation, and the low viscosity fracturing fluid could produce a large amount of filtration, which leads to the dissipation of hydraulic energy. In that case, we suggest improving fracturing fluid performance, such as adding polymers, to adjust fracturing fluid as a pseudoplastic liquid. For such a fluid, when flowing, it shows a low viscosity, which is conducive to the pressure conduction in fracture. When it leaks into the formation, as the flow rate decreases, the viscosity increases, which is beneficial to reduce filtration efficiency.

5. Conclusions

To analyze the propagation of hydraulic fractures in fracture-cavity carbonate formations, we established the hydraulic fracture propagation model in which random fractures and caves were considered. The model is determined by the minimum strain energy density method, allowing hydraulic fractures to expand along grid lines and complex interaction between hydraulic fractures and fracture-cavity systems. Based on this model, we analyzed the hydraulic fracture propagation in different fracture-cavity carbonate formations under fracturing parameters. From the results, we achieved the main conclusions as follows:

(1) For the cavernous carbonate formation, the propagation direction of hydraulic fractures is along the horizontal maximum *in-situ* stress; therefore, it is possible to communicate the caves located in the principal stress direction. However, when the fracture approached caves, the stress concentration could deflect it, shown as a repulsion interaction, which is not conducive to communication. The larger the cave is, the more obvious the repulsion is. We can make hydraulic fractures break through the repulsion and communicate with caves by adjusting fracturing parameters to improve the net pressure in fractures, such as increasing injection rate or reducing fluid viscosity.

(2) There is no doubt that the natural fractures around caves are conducive to hydraulic fractures communicating with fracture-cavity systems, as they can easily intersect natural fractures to build flow channels. It is not easy for hydraulic fractures to directly connect to caves due to the repulsion; therefore, it is a more sensible and efficient way to activate fractures around caves as much as possible.

(3) In this paper, we preliminarily discussed the hydraulic fracture propagation in fracture-cavity carbonate reservoirs and analyzed the differences of interactions between hydraulic fractures and caves or fracture-cavity systems. We raised four corresponding optimized fracturing modes according to different characteristics of the fracture-cavity formation, which provides feasibilities to improve the communication effect. However, due to the complexity of fracture-vuggy reservoirs, the interaction between hydraulic fractures and fracture-cavity systems are very complex, which have not been clearly revealed and deserve our further study.

Acknowledgments

The authors are grateful for the National Natural Science Foundation Program (No. 51874321).

References

Cheng, L., Luo, Z., Yu, Y., et al., 2019. Study on the interaction mechanism between hydraulic fracture and natural karst cave with the extended finite element method. Eng. Fract. Mech. 222, 106680. https://doi.org/10.1016/j.engfracmech.2019.106680.

Feng, Y., Jones, J.F., Gray, K.E., 2016. A review on fracture-initiation and-propagation pressures for lost circulation and wellbore strengthening. SPE Drill. Complet. 31 (2), 134–144. https://doi.org/10.2118/181747-PA.

Feng, Y., Li, X., Gray, K.E., 2017. Development of a 3D numerical model for quantifying fluid-driven interface debonding of an injector well. Int. J. Greenh. Gas Control 62, 76–90. https://doi.org/10.1016/j.ijggc.2017.04.008.

Ford, D., 1988. Characteristics of Dissolutional Cave Systems in Carbonate Rocks. Springer, New York. https://doi.org/10.1007/978-1-4612-3748-8_2.

Garipov, T.T., Karimi-Fard, M., Tchelepi, H.A., 2016. Discrete fracture model for coupled flow and geomechanics. Comput. Geosci. 20 (1), 149–160 doi:10.1007/s10596-015-9554-z.

Guo, T., Zhang, S., Zou, Y., et al., 2015. Numerical simulation of hydraulic fracture propagation in shale gas reservoir. J. Nat. Gas Sci. Eng. 26, 847–856. https://doi.org/10.1016/j.jngse.2015.07.024.

Karimi-Fard, M., Durlofsky, L.J., Aziz, K., 2003. An efficient discrete fracture model applicable for general purpose reservoir simulators. SPE Reservoir Simulation Symposium, doi:10.2118/79699-MS..

Keshavarzi, R., Mohammadi, S., 2012. A new approach for numerical modeling of hydraulic fracture propagation in naturally fractured reservoirs. SPE/EAGE European Unconventional Resources Conference and Exhibition, doi:10.2118/152509-MS.

Kremlev, A.N., Erokhin, G.N., Starikov, L.E., et al., 2008. Forecast of crack and cavernous reservoirs in carbonate, clay and magmatic rocks based on scattered seismic waves//3rd EAGE St. In: 3rd EAGE St. Petersburg International Conference and Exhibition on Geosciences-Geosciences: from New Ideas to New Discoveries. European Association of Geoscientists & Engineers cp-34-00006. doi:10.3997/2214-4609.20146800.

Li, Y., 2017. Development Theories and Methods of Fracture-Vug Carbonate Reservoirs. Academic Press.

Liu, B., Jin, Y., Chen, M., 2019a. Influence of vugs in fractured-vuggy carbonate reservoirs on hydraulic fracture propagation based on laboratory experiments. J. Struct. Geol. 124, 143–150. https://doi.org/10.1016/j.jsg.2019.04.007.

Liu, Y., Hou, J., Li, Y., et al., 2018. Characterization of architectural elements of Ordovician fractured-cavernous carbonate reservoirs, Tahe Oilfield, China. J. Geol. Soc. India 91 (3), 315–322. https://doi.org/10.1007/s12594-018-0856-3.

Liu, Z., Lu, Q., Sun, Y., et al., 2019b. Investigation of the influence of natural cavities on hydraulic fracturing using phase field method. Arabian J. Sci. Eng. 44 (12), 10481–10501. https://doi.org/10.1007/s13369-019-04122-z.

Liu, Z., Tang, X., Tao, S., et al., 2020. Mechanism of connecting natural caves and wells through hydraulic fracturing in fracture-cavity reservoirs. Rock Mech. Rock Eng. 53, 5511–5530. https://doi.org/10.1007/s00603-020-02225-w.

Loucks, R.G., 1999. Paleocave carbonate reservoirs: origins, burial depth modifications, spatial complexity, and reservoir implications. AAPG (Am. Assoc. Pet. Geol.) Bull. 83 (11), 1795–1834. https://doi.org/10.1306/E4FD426F-1732-11D7-8645000102C1865D.

Luo, C., Xue, F., Deng, X., et al., 2013. Cave system Analysis-An effective approach to predict hydrocarbons in cavernous carbonate reservoir. In: International Petroleum Technology Conference. European Association of Geoscientists & Engineers cp-350-00276. https://doi.org/10.2523/IPTC-16783-MS.

Luo, Z., Zhang, N., Zhao, L., et al., 2020. Interaction of a hydraulic fracture with a hole in poroelasticity medium based on extended finite element method. Eng. Anal. Bound. Elem. 115, 108–119. https://doi.org/10.1016/j.enganabound.2020.03.011.

Sesetty, V., Ghassemi, A., 2012. Simulation of hydraulic fractures and their interactions with natural fractures. 46th U.S. Rock Mechanics/Geomechanics Symposium, Chicago, Illinois, pp. 24–27. In: https://onepetro.org/ARMAUSRMS/proceedings-abstract/ARMA12/All-ARMA12/ARMA-2012-331/120661.

Sih, G.C., 1974. Strain-energy-density factor applied to mixed mode crack problems. Int. J. Fract. International Journal of fracture 10 (3), 305–321. https://doi.org/10.1007/BF00035493.

Tan, M.J., Gao, J., Wang, X.C., et al., 2011. Numerical simulation of the dual laterolog for carbonate cave reservoirs and response characteristics. Appl. Geophys. 8 (1), 79–85. https://doi.org/10.1007/s11770-011-0268-2.

Tan, P., Jin, Y., Hou, B., et al., 2019. Understanding hydraulic fracture propagation behavior in tight sandstone–coal interbedded formations: an experimental investigation. Petrol. Sci. 1 (16), 148–160. https://doi.org/10.1007/s12182-018-0297-z.

Tan, P., Pang, H., Zhang, R., et al., 2020. Experimental investigation into hydraulic fracture geometry and proppant migration characteristics for southeastern Sichuan deep shale reservoirs. J. Petrol. Sci. Eng. 184, 106517. https://doi.org/10.1016/j.petrol.2019.106517.

Tan, P., Jin, Y., Pang, H., 2021. Hydraulic fracture vertical propagation behavior in transversely isotropic layered shale formation with transition zone using XFEM-based CZM method. Eng. Fract. Mech. 248, 107707. https://doi.org/10.1016/j.engfracmech.2021.107707.

Wang, H., Tang, X., Luo, Z., et al., 2018. Investigation of the fracture propagation in fractured-vuggy reservoirs. In: The 52nd U.S. Rock Mechanics/Geomechanics Symposium. In: https://onepetro.org/ARMAUSRMS/proceedings-abstract/ARMA18/All-ARMA18/ARMA-2018-959/122698.

Wang, T., Chen, M., Wu, J., et al., 2021. Making complex fractures by re-fracturing with different plugging types in large stress difference reservoirs. J. Petrol. Sci. Eng. 201 (1), 108413. https://doi.org/10.1016/j.petrol.2021.108413.

Wei, S., Jin, Y., Xia, Y., 2020. Predict the mud loss in natural fractured vuggy reservoir using discrete fracture and discrete vug network model. J. Petrol. Sci. Eng. https://doi.org/10.1016/j.petrol.2020.107626, 107626.

Wei, S., Kao, J., Jin, Y., et al., 2021. A discontinuous discrete fracture model for coupled flow and geomechanics based on FEM. J. Petrol. Sci. Eng. (3), 108677. https://doi.org/10.1016/j.petrol.2021.108677.

Xia, Y., Jin, Y., Chen, M., et al., 2015. Hydrodynamic modeling of mud loss controlled by the coupling of discrete fracture and matrix. J. Petrol. Sci. Eng. 129, 254–267. https://doi.org/10.1016/j.petrol.2014.07.026.

Yang, R., Xu, P., Yue, Z., et al., 2016. Dynamic fracture analysis of crack–defect interaction for mode I running crack using digital dynamic caustics method. Eng. Fract. Mech. 161, 63–75. https://doi.org/10.1016/j.engfracmech.2016.04.042.

Yang, R.S., Ding, C.X., Yang, L.Y., et al., 2018. Hole defects affect the dynamic fracture behavior of nearby running cracks. Shock Vib. https://doi.org/10.1155/2018/5894356.